Journal of Materials Chemistry A

Accepted Manuscript

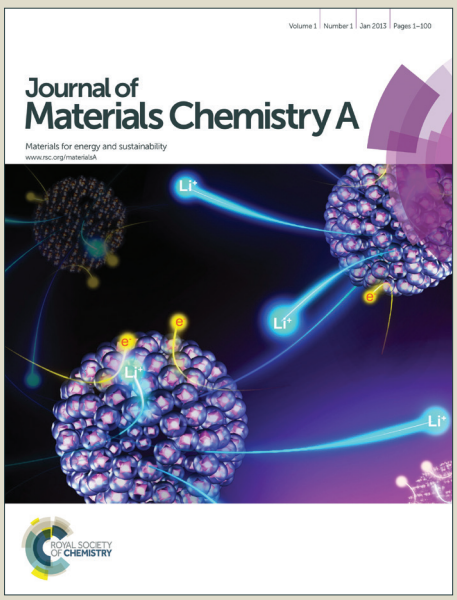

ROYAL SOCIETY OF CHEMISTRY

www.rsc.org/materialsA

Journal of Materials Chemistry A

ARTICLE

Composited Co_3O_4/Ag with Flower-Like Nanosheets Anchored on Porous Substrate as a High-Performance Anode for Li-Ion Batteries

Received 00th January 20xx,
Accepted 00th January 20xx

DOI: 10.1039/x0xx00000x

www.rsc.org/

Qin Hao,[a] Yang Yu,[b] Dianyun Zhao,[a] Caixia Xu[a]*

Co_3O_4/Ag composites with flower-like nanosheets anchored on porous substrate are easily fabricated through directly dealloying CoAgAl alloy in mild condition. Three different Ag content in the nanocomposites is conveniently achieved by means of controlling the feeding component of alloy precursor. Electrochemical measurements for lithium storage indicate that the incorporation of well-conductive Ag into Co_3O_4 dramatically enhances its cycling stability, especially at high current rates. Co_3O_4/Ag composite with 20 at.% Ag shows superior capacity and outstanding cycling stability, even at a high rate of 1000 mA g^{-1} for a long term of 1000 cycles. Meanwhile, it performs excellently in rate capability. With the advantages of unique performance and easy preparation, the Co_3O_4/Ag nanocomposite holds great application potential as an advanced anode material for lithium-ion batteries.

Introduction

With increasing concerns on fast depletion of fossil fuels and serious environmental problems, rechargeable lithium-ion batteries (LIBs) have been attracting more and more attentions in terms of high energy density and environment friendly operation.[1,2] However, the conventional carbonaceous anode material has a low theoretical capacity of 372 mA h g^{-1}, which cannot meet the ever growing requirements for next-generation high performance LIBs.[3] Therefore, considerable efforts have been dedicated to explore alternative anode materials with much higher capacities and long service life, such as Si- and Sn-based materials, transition metal oxides, etc.[4] Among various metal oxide materials, Co_3O_4 represents a promising class of anode material because of its high theoretical capacity of 890 mA h g^{-1}.[5] However, its low electronic conductivity and large volume change during the redox reaction process usually lead to a poor capacity retention over extended cycling period, thus hampering its practical use in LIBs. Therefore, how to ensure the large capacity accompanying with high reversibility for Co_3O_4 anode remains a great challenge for its practical application in LIBs.

At present, one of effective strategies to improve the electrochemical performance of Co_3O_4 anodes is to engineer specific nanostructured materials with favourable size, structure, and morphology.[6-12] It has been demonstrated that nanomaterials are beneficial for shortening the Li^+ diffusion distance, improving the electroactivity, and relieving the absolute volume variation during the discharging-charging process, etc. Meanwhile, microscaled structure has the merits itself compared with nano-electrodes. For instance, they are less susceptible to agglomerate and can be packed more densely on the current collector against collapse.[13] Therefore, it is essential to make good use of the advantages of nano-sized and micro-sized structure to design and fabricate high-performance Co_3O_4 anode materials. Another effective strategy is the introduction of well-conductive species to form composite with Co_3O_4 aiming to optimize the electric connectivity of electrode material.[14-17] For example, Kim group[15] employed graphene layers to enhance the electronic conductivity and Li ion transfer of Co_3O_4 electrode, thus ameliorating its lithium storage properties.

Inspired by the aforementioned statement and recent work, herein we focus on engineering the morphology coupled with the advantages of microscaled and nanoscaled materials as well as incorporating well conductive Ag species to achieve the much higher performance over Co_3O_4 anode. Until now, a number of methods have been employed to prepare metal oxides, such as sol-gel, chemical vapor deposition, hydrothermal and solvothermal methods, etc.[18-21] However, these methods are relatively complicated, which usually involve the use of high-temperature, multi-step operation, and careful control for the whole operation conditions, etc. Therefore, it is necessary to develop a simple and convenient technique to prepare the desirable composites in high throughput under mild conditions.

Address: [a]School of Chemistry and Chemical Engineering, University of Jinan, Jinan, 250022, China.
Fax: +86-531-82765969
Tel: +86-531-89736103
E-mail: chm_xucx@ujn.edu.cn
[b]Shandong Product Quality Inspection Research Institute, Jinan, 250102, China.
Electronic Supplementary Information (ESI) available: [The cross-sectional SEM and CV curves of the Co_3O_4/Ag electrode dealloyed from $Co_{12}Ag_3Al_{85}$ alloy , XPS spectra of Co 2p and Ag 3d for the fresh Co_3O_4/Ag dealloyed from $Co_{13}Ag_2Al_{85}$ and $Co_{14}Ag_1Al_{85}$ alloys]. See DOI: 10.1039/x0xx00000x

A dealloying method was developed by our group to prepare nanostructured metal oxides owing to the spontaneous oxidation of the reactive metal atoms by oxygen-containing species, such as Co_3O_4, Mn_3O_4.[22-24] In general, this dealloying strategy exhibits evident advantages of simple processing, nearly absolute yield, and flexibility for large-scale synthesis. Herein, we report a simple preparation of Co_3O_4/Ag composites with hierarchical micro-/nano-structure and different Ag contents through dealloying the well-designed CoAgAl alloys in NaOH solution. Owing to the unique hierarchical structure and improved conductivity, Co_3O_4/Ag composite exhibits much enhanced cycling stability with the increase of Ag content, especially at high current rates. With the advantages of unique performance and easy preparation, the Co_3O_4/Ag composite demonstrates promising application potential for lithium storage.

Experimental Section

Sample preparation

All reagents (purchased from Shanghai Sinopharm Chemical Reagent Ltd. Co of China) were analytical grade and used without further purification. $Co_{12}Ag_3Al_{85}$, $Co_{13}Ag_2Al_{85}$ and $Co_{14}Ag_1Al_{85}$ alloy foils were prepared through refining Co, Ag and Al with the designed atomic percentages in an arc-furnace and further melt-spinning at 1600r under a protective argon atmosphere. Subsequently, the alloy foils were etched in 1 M NaOH solutions at room temperature, and the products were washed several times with ultra-pure water (18.2 M Ohm) and dried at room temperature in air.

Characterization

The crystal structure and morphology of products were characterized by X-ray diffraction (XRD, Bruker D8 advanced X-ray diffractometer using Cu Kα radiation at a step rate of 0.04 $°s^{-1}$) and Field Emission scanning electron microscopy (SEM, JEOL JSM-7600F) with an energy-dispersive X-ray spectrometer (EDS). Elemental mapping was obtained using a FEI QUANTA FEG250 scanning electron microscope equipped with an INCA Energy X-MAX-50 X-ray spectroscopy analyzer. X-ray photoelectron spectrometer (XPS) was performed on a Thermo Scientific ESCALAB 250 X-ray photoelectronic spectrometer, employing a monochromatized Mg Kα X-ray as the excitation source and choosing C1s (284.60 eV) as the reference line.

Electrochemical tests

The electrochemical performance were measured using CR 2032 coin-type cells, which employed cellgard 2300 and lithium metal foil as separator and reference electrode, respectively. The electrolyte was the solution of 1 mol L^{-1} $LiPF_6$ dissolved in ethylene carbonate (EC)-dimethyl carbonate (DMC)-ethylene methyl carbonate (EMC) (volume ratio is 1:1:1). Co_3O_4/Ag powders, carboxymethyl cellulose (CMC) and acetylene black in a weight ratio of 7.5:1.5:1.5 were mixed in ultrapure water to prepare slurry, which was further coated onto a piece of Cu foil and dried under vacuum at 80 °C for 8 h to obtain the working electrodes. Subsequently, the cells were assembled in an Ar filled humidity-free glove box. For a long-term galvanostatical tests, the cells were discharged and charged between 0.01 and 3 V using a NEWARE BTS 5 V-5 mA computer-controlled galvanostat (Shenzhen, China) at different current density. Electrochemical impedance spectroscopy (EIS) was conducted with a Princeton Applied Research spectrometer by applying an alternating current voltage of 10 mV in the frequency range from 0.01 to 100 kHz.

Results and Discussions

In this work, CoAgAl ternary alloy was selected as the source alloy owing to the rich supply and relatively low price of Al. Meanwhile, in order to understand the effect of well conductive Ag on the lithium storage performance of Co_3O_4 anode, CoAgAl alloys with three different component ratios ($Co_{12}Ag_3Al_{85}$, $Co_{13}Ag_2Al_{85}$, $Co_{14}Ag_1Al_{85}$) were designed for comparison. In addition, we selected $Co_{12}Ag_3Al_{85}$ alloy as a representative to investigate the effect of dealloying conditions on the crystal structure and morphology of product. Considering the amphoteric property of Al, NaOH solution was selected as the electrolyte to selectively remove Al atoms as well to avoid the dissolution of Co and Ag.

We reported earlier that once Al in the CoAl binary alloy was selectively etched by NaOH, the residual Co atoms would undergo spontaneous oxidation at the metal/electrolyte interface to form Co_3O_4.[24] Therefore, XRD measurement was first carried out to investigate the crystal structure of the fresh product obtained by etching $Co_{12}Ag_3Al_{85}$ alloy in 1 M NaOH solution for 10 h at room temperature. As presented in Fig. 1a, a set of diffraction peaks can be indexed to Ag phase but no peak can be assigned to Co_3O_4 phase. In order to further understand its structural composition, the fresh sample was crystallized through annealing at 450 °C for 5 h under N_2 atmosphere. As demonstrated in Fig. 1b, the annealed sample is composed of two phases of Co_3O_4 and Ag, indicating the presence of an amorphous state of Co_3O_4 in the fresh sample, which is in keeping with the result described in our early work.[24] XPS technique was further used to examine the surface structures and properties of the freshly dealloyed sample. Fig. 1c shows the XPS spectra for Co 2p core level region, where strong Co 2p peaks around 780.0 and 795.3 eV and weak shoulder peaks at higher binding energies can be assigned to Co_3O_4 material.[25] Fig. 1d further shows the XPS spectra of Ag 3d region, in which the peaks around 368.4 and 374.4 eV can be attributed to metallic Ag.[26] According to the above analysis, the freshly dealloyed sample should be characterized to be Co_3O_4/Ag composite. In addition, the chemical reaction equations of the dealloying process are given as the following equations (1-2).

$$Al + NaOH + H_2O \longrightarrow NaAlO_2 + H_2 \quad (1)$$

$$Co + O_2 \xrightarrow{OH^-} Co_3O_4 \quad (2)$$

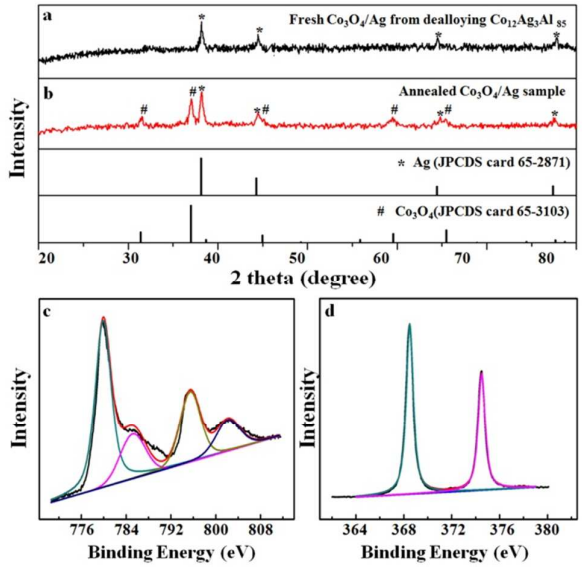

Fig. 1. The XRD patterns of (a) fresh Co_3O_4/Ag sample prepared through etching $Co_{12}Ag_3Al_{85}$ alloy in 1 M NaOH solution for 10 h, (b) annealed product obtained by annealing the fresh Co_3O_4/Ag at 450 °C for 5 h under N_2; XPS spectra of (c) Co 2p and (d) Ag 3d for the fresh Co_3O_4/Ag.

SEM was used to investigate the microstructure of the fresh Co_3O_4/Ag sample prepared through immersing $Co_{12}Ag_3Al_{85}$ alloy in 1 M NaOH solution for 10 h. It is clearly observed from Fig. 2a that the sample consists of a large quantity of flower-like structure, which are well assembled by interlaced nanosheets with the thickness about 100 nm. In order to gain much more detailed structural formation of the dealloying product, two other SEM images with higher magnification are given in Fig. 2b & 2c. Interestingly, it is found that those flowers anchor on a nanoporous substrate with the pore size about 150 nm, which makes the sample connective to form a hierarchical structure in micrometer-scale. In addition, a cross-sectional SEM image (Fig. S1) further exhibits the unique structure. The uniform bicontinuous nanoporous substrate demonstrates that NaOH solution had penetrated the whole sample in all dimensions upon dealloying. Recently, many researchers have reported that designing the electrode materials with micro-/nano-structures can effectively optimize their lithium storage properties owing to the incorporation of the advantages of micro- and nano-materials.[8-10] Therefore, combining the three dimensional interconnected network structure with flower-like nanosheets, the micro-sized Co_3O_4/Ag sample is expected to exhibit encouraging performance as an anode material for LIBs. Subsequently, element mapping results of the Co_3O_4/Ag composite are displayed in Fig. 2d-f to understand the location and identity of atoms. As observed, three elements of Co, Ag and O disperse homogenously, indicating the uniform inter-crossed growth of both Co_3O_4 and Ag in the product. Meanwhile, EDS is used to confirm its composition with CoAgAl source alloy included for comparison. Fig. 2g first gives the EDS result of the designed $Co_{12}Ag_3Al_{85}$ alloy. The atomic percentage of Co, Ag, and Al is much closing to our initial feeding ratio in the refining process. Fig. 2h further presents the data for Co_3O_4/Ag product. The atomic ratio between Co and Ag upon dealloying is about 4:1, which is highly consistent with the initial feeding ratio between Co and Ag in $Co_{12}Ag_3Al_{85}$ source alloy, indicating the good control of the resulted component.

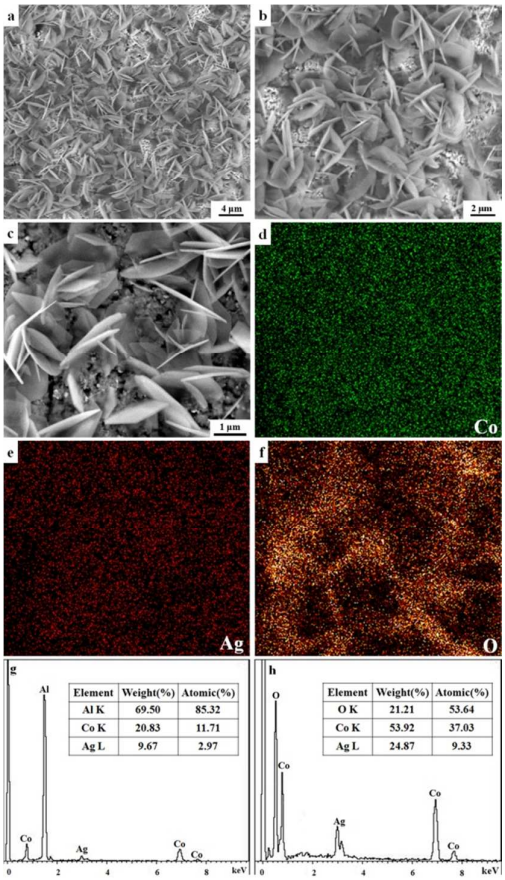

Fig. 2. (a-c) SEM images, (c) element mapping of (d) Co, (e) Ag, (f) O, (h) EDS compositional analysis of the Co_3O_4/Ag composite prepared through dealloying $Co_{12}Ag_3Al_{85}$ alloy in 1 M NaOH solution for 10 h, EDS results of (g) $Co_{12}Ag_3Al_{85}$ alloy and (h) Co_3O_4/Ag composite.

To give insight into the formation and evolution of this unique Co_3O_4/Ag structure, the resulted samples at different dealloying stages were monitored. Fig. 3a gives the SEM image of a typical $Co_{12}Ag_3Al_{85}$ alloy foil and the digital photograph (inset in Fig. 3a), which shows its silvery luster feature with smooth surface. After a short corrosion period of 2 h (Fig. 3b), the dense surface of alloy became loose to from a porous structure, and some ultrathin sheets became growing on the surface. Subsequently, the sizes of those nanosheets gradually became larger with increasing the corrosion time. When dealloying for 5 h (Fig. 3c), abundant nanosheets had formed on the nanoporous substrate, parts of which self-assembled to a flower-like structure. However, the size of those nanosheets were not uniform at this stage. If the corrosion time was extended for 10 h (Fig. 3d), lots of flowers assembled by the interlaced nanosheets uniformly anchored on the nanoporous substrate. According to the observations above, the whole growth procedure of the unique Co_3O_4/Ag structure can be illustrated by a scheme as Fig. 4. First, CoAgAl alloy foils with

the designed atomic ratio are dealloyed in NaOH solution (Fig. 4a). Owing to the selective dissolution of Al atoms in NaOH solution, the alloy foil becomes to form a nanoporous structure. Meanwhile, the remained more reactive Co atoms undergo a simultaneous oxidation by OH^- and/or oxygen species at the metal/electrolyte interface to form Co_3O_4 material. As the dealloying process going on, the Co and Ag atoms continue to diffuse and grow in the alkaline condition. During dealloying, some ultrathin sheets continuously grow on the nanoporous surface (Fig. 4b), which become larger in size and self-assemble to build the flower-like structure on the nanoporous substrate (Fig. 4c&d).

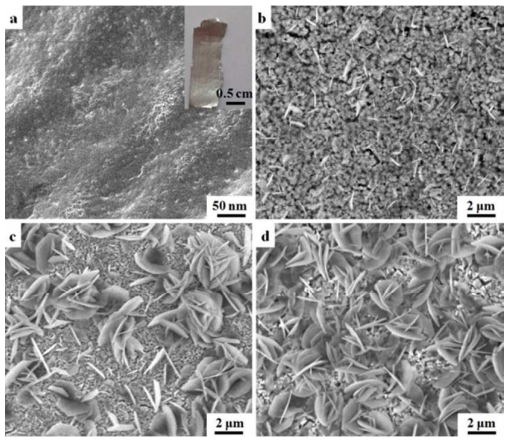

Fig. 3. SEM images of the samples obtained through etching $Co_{12}Ag_3Al_{85}$ alloy in 1 M NaOH solution for (a) 0, (b) 2, (c) 5, (d) 10 h.

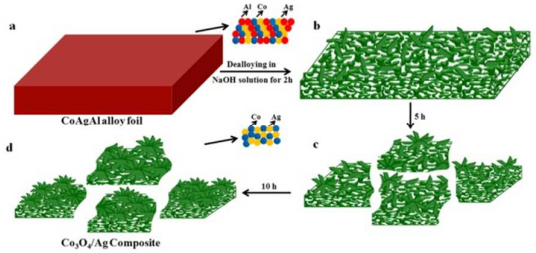

Fig. 4. Schematic fabrication of the unique Co_3O_4/Ag structure.

Meanwhile, to investigate the influence of incorporating well conductive Ag on the electrochemical properties of Co_3O_4 electrode, Co_3O_4/Ag nanocomposites with two other Ag contents were also fabricated by dealloying the designed $Co_{13}Ag_2Al_{85}$ and $Co_{14}Ag_1Al_{85}$ alloys under the same corrosion condition. For convenience, the fresh products dealloyed from $Co_{12}Ag_3Al_{85}$, $Co_{13}Ag_2Al_{85}$ and $Co_{14}Ag_1Al_{85}$ alloys were labelled as C1, C2, and C3, respectively. XPS spectra are first presented in Fig. S2 to understand the surface structures and properties of C2 and C3, which confirm that both samples are also Co_3O_4/Ag composites. In addition, the SEM images (Fig. 5a&5b) further demonstrate that they exhibit similar structure feature as C1. Finally, EDS compositional analysis is further employed to examine the controllability on the component of resulted product. As indicated in Fig. 5b&5d, the atomic ratios between Co and Ag in C2 and C3 are 6.5:1 and 14.1:1, which are close to the initial feeding ratio in $Co_{13}Ag_2Al_{85}$ and $Co_{14}Ag_1Al_{85}$ alloys, respectively. The atom ratios of Ag against the total metal atoms are calculated to be 20, 13, and 7 at.% in C1, C2, and C3.

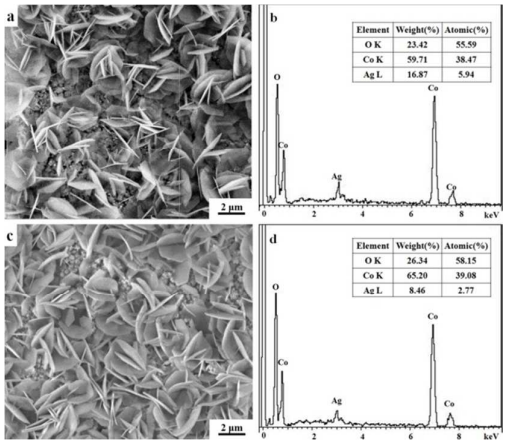

Fig. 5. SEM images and EDS analysis of Co_3O_4/Ag composites obtained by dealloying (a&b) $Co_{13}Ag_2Al_{85}$ and (c&d) $Co_{14}Ag_1Al_{85}$ alloys in 1 M NaOH solution for 10 h.

The successful fabrication of three Co_3O_4/Ag composites with similar structure but different Ag content provides good opportunity to investigate the influence of Ag on the lithium storage performance of Co_3O_4 anode. C1, C2, and C3 samples were used as anode materials to carry out the galvanostatic discharging-charging tests. As shown in Fig. 6a, C1 delivers a lowest initial capacity of 936.1 mA h g^{-1} due to the highest Ag content among the three samples. During the earlier period, all electrodes exhibit declining tendencies in capacity. Subsequently, the difference on their cycling durability becomes more and more obvious. In the case of C3 anode, the capacity degradation persistently exists in the whole cycling period, and the capacity remains only 45.6 % at 500th cycle. However, it is evident that the capacity durability of electrode increases with an increase of Ag content in sample. Especially for C1 anode, the capacity is highly stable at about 580 mA h g^{-1} in the later cycling process, exhibiting a capacity retention up to 61.5% at 500th cycle against the initial capacity. In addition, the corresponding coulombic efficiencies (CE, the ratio between the charge and discharge capacities) are further calculated to better investigate their electrochemical performance. As demonstrated in Fig. 6b, the initial CEs are 84.3 %, 80.4 %, and 77.6 % for C1, C2, and C3 electrodes, respectively, indicating that the incorporation of Ag is beneficial to improve the initial capacity reversibility of Co_3O_4 electrode. Subsequently, the CEs for three electrodes all increase sharply above 93 % at the second cycle, and maintained between 98-100 % in the following several hundred cycles.

An excellent cycling stability at high current density is significant for the practical application of an advanced electrode material. Therefore, we further compared the electrochemical performance of the three Co_3O_4/Ag electrodes at a high rate of 1000 mA g^{-1} for a long test period of 1000 cycles. As shown in Fig. 6c, three anodes exhibit distinctively different cycling stabilities. C3 delivers a highest initial

capacity of 1008.6 mA h g^{-1}, but the capacity exhibits a sustained downward trend and drops to only 166.1 mA h g^{-1} at 1000th cycle, corresponding to a low capacity retention of 16.5 %. Similarly, a capacity fading phenomenon is also observed for C2 electrode, however, the decay rate is much slower compared with that of C3. At the end of the cycling test, C2 presents an enhanced capacity retention of 29.9 % against its initial capacity. In comparison, C1 demonstrates a highest electrochemical reversibility. When the discharging-charging progress is lasted for 30 cycles, the capacity of C1 decreases from 904.7 mA h g^{-1} at 1st cycle to 520.6 mA h g^{-1}. However, the electrode performs stably during the rest long cycling period. At 1000th cycle, C1 exhibits the capacity retention of 51.7 % against the initial capacity and 90.0 % against the capacity at 31th cycle.

In order to present a more clear comparison of the electrochemical performance of three electrodes both at 500 and 1000 mA g^{-1}, their corresponding capacities, CEs and capacity retentions are summarized in Table 1. As presented in Table 1, increasing the Ag content will decrease the initial capacity of electrode material, however, it is beneficial to enhance the initial CE and cycling reversibility, especially at high current rate. Such an optimization should be attributed to the enhanced electric conductivity and a decreased inner resistance of electrode material by well conductive Ag.

For directly proving the contribution of Ag on the conductivity of electrode, electrochemical impedance spectroscopy (EIS) measurements for the three electrodes were measured at an open circuit voltage state using fresh cells. As illustrated by the Nyquist profiles in Fig. 6d, each plot consists of a depressed semicircle in the high-frequency region attributing to the charge-transfer impedance of cell, and a sloping line in low-frequency region representing the mass transfer of Li^+.[6,26] It is found that the obvious difference among three samples lies in the diameter of the semicircle, which shows lowering trend with the increase of Ag content in sample. In other words, the charge transfer of Co_3O_4 electrode became easier due to the incorporation of well conductive Ag, thus leading to a better electrochemical performance. This is in accordance with the results of the reported similar materials.[28] In addition, in order to further understand the electrochemical details of the lithium insertion-extraction process of Co_3O_4/Ag composite, cyclic voltammetric (CV) test was carried out between 0.01 and 3 V at a scan rate of 0.1 mV s^{-1}. As shown in Fig. S3, the cathodic and anodic current peaks indicate a multistep electron capture and loss procedure during the redox reaction, which are similar with those reported in other literatures.[29,30] The higher current peak intensity in the first cycle reveals a faster kinetics for the phase transformation of cobalt and the formation of the solid electrolyte interphase film.[31] In the following two cycles, the shape and intensity of the current peaks remain similar, suggesting the reversibility of Co_3O_4/Ag anode.

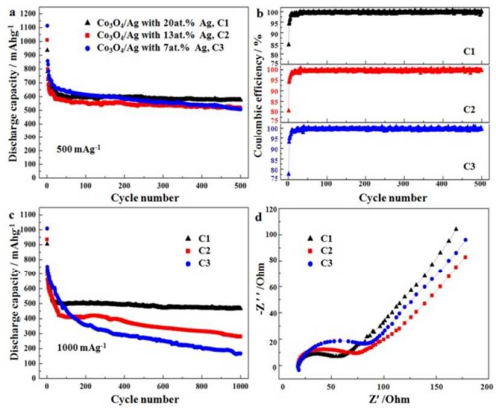

Fig. 6. The (a&c) cycling behaviour, (b) coulombic efficiency, and (d) Nyquist plot of the fresh C1, C2, and C3 samples [current rate: (a&b) 500 mA g^{-1}, (c) 1000 mA g^{-1}].

Table 1. Discharge capacities, CEs and capacity retentions of C1, C2 and C3 anodes at different rates.

Sample	At 500 mA g^{-1} for 500 cycles				At 1000 mA g^{-1} for 1000 cycles			
	Initial capacity	Last capacity	Initial CE	Capacity retention	Initial capacity	Last capacity	Initial CE	Capacity retention
C1	936.1	575.6	84.3	61.5%	904.7	467.3	79.7	51.7%
C2	1009.3	517.6	80.4	51.3%	935.2	279.3	78.5	29.9%
C3	1113.6	507.4	77.6	45.6%	1008.6	166.1	75.8	16.5%

Base on the above investigation, C1 exhibits the most satisfactory specific capacity and best cycling stability among three samples. In order to obtain the greater understanding about its application potential as an advanced anode material for LIBs, we further evaluate its power capability at different current densities. Fig. 7a first presents its performance tested in discrete steps from 50 to 500 mA g^{-1}. It is observed that C1 shows very good cycling reversibility, holding the average capacities of about 780, 700, 645, and 600 mA h g^{-1} at the rates of 50, 100, 200, and 500 mA g^{-1}, respectively. When the current rate is set back to 50 mA g^{-1}, a capacity of ~ 750 mA h g^{-1} is well recovered, which reaches up to 97 % of the capacity at the last cycle at previous rate of 50 mA g^{-1}. In addition, the rate performance of C1 is also evaluated at much higher current rates from 500 to 3000 mA g^{-1} (Fig. 7b). As expected, C1 electrode exhibites a good rate capability. Even at 2000 and 3000 mA g^{-1}, C1 delivers the stable reversible capacities of about 460 and 390 mA h g^{-1}, respectively. If the current is reverted to 500 mA g^{-1}, the capacity returns to ~ 595 mA h g^{-1} with 86.2 % of the capacity recovered at the initial 500 mA g^{-1}. The superiority of Co_3O_4/Ag nanocomposite in high power capability is further visualized, which may be attributed to the following reasons. First, the unique Co_3O_4/Ag composite possesses the advantages of both nanosized building blocks and microsized assemblies towards lithium storage, thus exhibiting enhanced structure stability and

charge-transport capabilities upon cycling.[32-34] Second, the additive Ag acts as an efficient buffering and conducting matrix, which accommodates volume changes and improves the electrical conductivity. Finally, the unique structure with high porosity can allow the free expansion of Co_3O_4 with alleviative mechanical constrain during the discharging-charging process, meanwhile providing rich channels for the transport of Li^+ ions and electrons. [6-11]

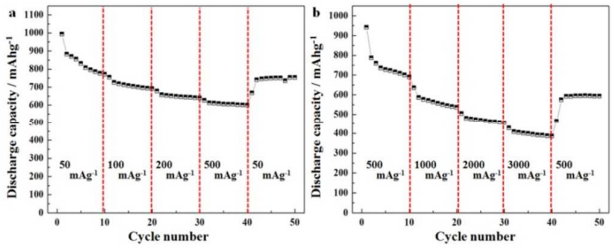

Fig. 7. The rate performance of the fresh C1 sample [rate: (a) 50-500 and (b) 500-3000 mA g^{-1}].

Conclusions

Composited Co_3O_4/Ag with flower-like nanosheets anchored on porous substrate was easily fabricated through one-step dealloying CoAgAl alloy in mild condition. By well designing the initial feeding component of CoAgAl precursor, Co_3O_4/Ag nanocomposites with three different Ag content were conveniently prepared in high through-put. Owing to the incorporation of well-conductive Ag, Co_3O_4/Ag composite exhibited much enhanced cycling stability, especially at high current rates. Especially for the composite with 20 at.% Ag, it exhibited high capacity and outstanding cycling stability, even at a high rate of 1000 mA g^{-1} for 1000 cycles. Meanwhile, it performed excellently in rate capability. With the advantages of unique performance and easy preparation, the as-made Co_3O_4/Ag nanocomposite holds great application potential for lithium storage.

Acknowledgements

This work was also supported by the National Science Foundation of China (21401074, 21271085) and Shandong Province (ZR2014BP013).

References

1 J. B. Goodenough and Y. Kim, *Chem. Mater.*, 2010, **22**, 587-603.
2 M. Armand and J. M. Tarascon, *Nature*, 2008, **451**, 652-657.
3 J. J. Vilatela and D. Eder, *ChemSusChem*, 2012, **5**, 456-478.
4 R. Mukherjee, R. Krishnan, T. M. Lu and N. Koratkar, *Nano Ener.*, 2012, **1**, 518-533.
5 W. Y. Li, L. N. Xu and J. Chen, *Adv. Funct. Mater.*, 2005, **15**, 851-857.
6 W. J. Hao, S. M. Chen, Y. J. Cai, L. Zhang, Z. X. Li and S. J. Zhang, *J. Mater. Chem. A*, 2014, **2**, 13801-13804.
7 X. H. Wang, Y. Fan, R. A. Susantyoko, Q. Z. Xiao, L. M. Sun, D. Y. He and Q. Zhang, *Nano Ener.*, 2014, **5**, 91-96.
8 B. Zhang, Y. B. Zhang, Z. Z. Miao, T. X. Wu, Z. D. Zhang and X. G. Yang, *J. Power Source*, 2014, **248**, 289-295.
9 G. Y. Huang, S. M. Xu, S. S. Lu, L. Y. Li and H. Y. Sun, *ACS Appl. Mater. Interfaces*, 2014, **6**, 7236-7243.
10 B. Wang, X. Y. Lu and Y. Y. Tang , *J. Mater. Chem. A*, 2015, **3**, 9689-9699.
11 L. Yu, L. Zhang, H. B. Wu, G. Q. Zhang and X. W. Lou, *Energy Environ. Sci.*, 2013, **6**, 2664-2671.
12 J. S. Chen, T. Zhu, Q. H. Hu, J. J. Gao, F. B. Su, S. A. Qiao and X. W. Lou, *ACS Appl. Mater. Interfaces*, 2010, **2**, 3628-3635.
13 Y. G. Wang, H. Q. Li, P. He, E. Hosono and H. S. Zhou, *Nanoscale*, 2010, **2**, 1294-1305.
14 L. Peng, Y. Y. Feng, Y. J. Bai, H. J. Qiu and Y. Wang, *J. Mater. Chem. A*, 2015, **3**, 8825-8831.
15 S. Abouali, M. A. Garakani, B. Zhang, H. Luo, Z. L. Xu, J. Q. Huang, J. Q. Huang and J. K. Kim, *J. Mater. Chem. A*, 2014, **2**, 16939-16944.
16 Y. M. Kang, K. T. Kim, J. H. Kim, H. S. Kim, P. S. Lee, J. Y. Lee, H. K. Liu and S. X. Dou, *J. Power Source*, 2004, **133**, 252-259.
17 B. B. Wang, G. Wang and H. Wang, *Mater. Lett.*, 2014, **122**, 186-189.
18 D. Fang, L. C. Li, W. L. Xu, G. Z. Li, G. Li, N. F. Wang, Z. P. Luo, J. Xu, L. Liu and C. L. Huang, *J. Mater. Chem. A*, 2013, **1**, 13203-13208.
19 H. Y. Liang, J. M. Raitano, L. H. Zhang and S. W. Chan, *Chem. Commun.*, 2009, **48**, 7569-7571.
20 J. Ma and A. Manthiram, *RSC Adv.*, 2012, **2**, 3187-3189.
21 C. Li, T. Q. Chen, W. J. Xu, X. B. Lou, L. K. Pan, Q. Chen and B. W. Hu, *J. Mater. Chem. A*, 2015, **3**, 5585-5591.
22 C. X. Xu, R. Y. Wang, Y. Zhang and Y. Ding, *Nanoscale*, 2010, **2**, 906-909.
23 Q. Hao, J. P. Wang and C. X. Xu, *J. Mater. Chem. A*, 2014, **2**, 87-93.
24 Q. Hao, M. H. Li, S. Z. Jia, X. Y. Zhao and C. X. Xu, *RSC Adv.*, 2013, **3**, 7850-7854.
25 D. Barreca, C. Massignan, S. Daolio, M. Fabrizio, C. Piccirillo, L. Armelao and E. Tondello, *Chem. Mater.*, 2001, **13**, 588-593.
26 Z. M. Liu, N. Q. Zhang, Z. J. Wang and K. N. Sun, *J. Power Sources*, 2012, **205**, 479-482.
27 Z. Q. Li, B. Li, L. W. Yin and Y. X. Qi, *ACS Appl. Mater. Interfaces*, 2014, **6**, 8098-8107.
28 J. X. Wang, Q. B. Zhang, X. H. Li, D. G. Xu, Z. X. Wang, H. J. Guo and K. L. Zhang, *Nano Ener.*, 2014, **6**, 19-26.
29 S. L. Chou, J. Z. Wang, H. K. Liu and S. X. Dou, *J. Power Sources*, 2008, **182**, 359-364.
30 C. Wang, D. L. Wang, Q. M. Wang and L. Wang, *Electrochim. Acta*, 2010, **55**, 6420-6425.
31 P. Zhang, Z. P. Guo, Y. D. Huang, D. Z. Jia and H. K. Liu, *J. Power Sources*, 2011, **196**, 6987-6991.
32 P. Wu, H. Wang, Y. W. Tang, Y. M. Zhou and T. H. Lu, *ACS Appl. Mater. Interfaces*, 2014, **6**, 3546-3552.
33 Q. Y. Zhu, P. Wu, J. J. Zhang, W. Y. Zhang, Y. M. Zhou, Y. W. Tang and T. H. Lu, *ChemSusChem*, 2015, **8**, 131-137.
34 J. P. Li, P. Wu, Y. W Tang, X. L. Xu, Y. M. Zhou, Y. Chen and T. H. Lu, *CrystEngComm*, 2013, **15**, 10340-10345.

Table of Contents

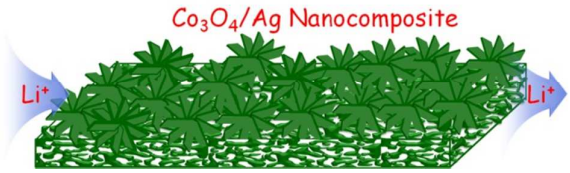

Co_3O_4/Ag nanocomposites with hierarchical micro-/nano-structure and controllable component are easily fabricated by etching well-designed CoAgAl alloys in NaOH solution, which perform excellently as anode materials for lithium storage.